# Conformation and Interactions of Polystyrene and Fullerenes in Dilute to Semidilute Solutions

**ARTICLE** *in* MACROMOLECULES · SEPTEMBER 2014

Impact Factor: 5.8 · DOI: 10.1021/ma501015s

Macromolecules

Article

pubs.acs.org/Macromolecules

# Conformation and Interactions of Polystyrene and Fullerenes in Dilute to Semidilute Solutions

Rajeev Dattani,[†,‡] Rolf Michels,[§] Alisyn J. Nedoma,[†,‡] Ralf Schweins,[∥] Paul Westacott,[†,⊥] Klaus Huber,[§] and João T. Cabral*[,†,‡]

[†]Centre for Plastic Electronics, [‡]Department of Chemical Engineering, and [⊥]Materials Department, Imperial College London, London SW7 2AZ, United Kingdom

[§]Physikalische Chemie, Universität Paderborn, 33098 Paderborn, Germany

[∥]Institut Laue-Langevin, DS/LSS, F-38042 Grenoble, France

Supporting Information

**ABSTRACT:** We report the polymer conformation and fullerene aggregation in a ternary system containing polystyrene, $C_{60}$, and toluene measured by small angle neutron, static, and dynamic light scattering. We investigate polymer concentrations across the dilute and semidilute regime for five polymer molecular weights ($M_w$ = 20 kg/mol to 1 Mg/mol), and fullerene concentrations below and above its miscibility threshold in toluene. We find that the polymer radius of gyration ($R_g^{poly}$), hydrodynamic radius ($R_h$), and the mixture correlation length ($\xi$) remain unchanged upon addition of $C_{60}$. The miscibility of $C_{60}$ in toluene, however, decreases upon addition of polystyrene forming aggregates with a time-dependent radius on the order of 100 nm, and this effect is amplified with increasing polymer $M_w$. Our findings are relevant to the solution processing of organic photovoltaics, which generally require the effective solubilization of fullerene derivatives and polymer pairs in this concentration range.

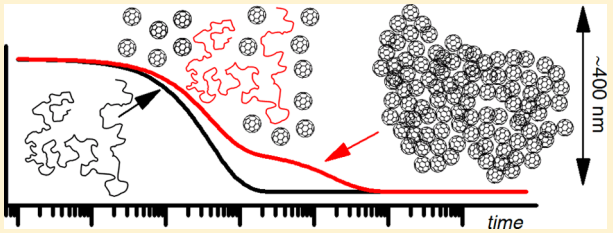


## INTRODUCTION

The addition of colloids, nanoparticles (NPs), or small molecules to polymers has been studied for a wide range of applications ranging from paints[1] to self-healing networks[2] and organic electronics.[3] Understanding the miscibility and conformation of polymer/NP solutions is key to the solution processing of nanocomposite materials. It is conceivable that sufficiently small NPs may behave as solvents or colloids in solution, in the so-called protein limit and affect polymer dimensions and phase behavior, depending on the polymer−NP interactions and their relative concentrations in solution.

Polymer/colloid/solvent mixtures are commonly discussed within two limits: the colloid limit (CL) and the protein limit (PL), usually defined by the relative magnitudes of radius of gyration of the polymer $R_g^{poly}$ and the radius of the colloid, $R_C$: $R_g^{poly} \ll R_C$ in CL, and $R_g^{poly} \gg R_C$ in PL.[4] The Asakura−Oosawa model provides a framework for understanding polymer/colloid systems in the CL.[5,6] Fullerenes have a radius ≈0.35 nm and polymer/fullerene solutions are thus generally expected to be in the PL, for which theoretical predictions are less clear.[7] De Gennes[8] predicted dispersibility in the case of weak interaction potentials between colloids with $R_C < \xi$, where $\xi$ is the correlation length in the semidilute regime, and Odijk[9] corroborated later that no phase separation should be expected between hard small spheres and much larger chains. Polymer coils, on the other hand, have been predicted to start to collapse in solution upon addition of colloids once the size ratio ($R_g^{poly}/R_C$) enters the PL.[7,10] Inspired by these predictions, Kramer et al.[11,12] experimentally studied three systems in the PL−polystyrene chains mixed with octa-*n*-propylsilsesquioxane (SILS) ($R_C$ = 0.7 nm), cross-linked poly(ethyl methacrylate) ($R_C$ = 8−42 nm), or hydroxyl functionalized silica nanoparticles ($R_C$ = 11 nm). Significant (≈50%) coil contraction was found in the presence of high enough (≳8 wt %) colloid concentration by means of viscosimetry, light scattering, and small angle neutron scattering.[12] In addition, increasing polymer concentration was found to decrease the solubility of SILS particles; expelled from the polymer coils, the effective SILS concentration increased in the solution bulk phase, resulting in SILS crystallization (as indeed found in proteins,[13] from which the term PL is derived). The addition of NPs to polymer melts has also attracted considerable research and controversy, in part due to the variable dispersion quality of nanocomposites.[14]

In this paper, we investigate $C_{60}$, a carbon allotrope,[15] and polystyrene (PS) in solution. $C_{60}$ can be found as a single molecule in solution and can cluster into colloidal particles on the order of 100s nm or crystallize, depending on solvent quality.[16] We select toluene as a good solvent for PS and also comparatively good for $C_{60}$, which is miscible up to 0.32 wt

Received: May 15, 2014
Revised: July 12, 2014

   dx.doi.org/10.1021/ma501015s | Macromolecules XXXX, XXX, XXX−XXX

%.[17] We evaluate two main aspects of polymer/fullerene solutions: the effect of $C_{60}$ on the conformation of PS chains and the effect of PS on miscibility and aggregation of $C_{60}$. We employ static light scattering (SLS), dynamic light scattering (DLS), and small angle neutron scattering (SANS) to quantify the miscibility, polymer $R_g^{poly}$, polymer hydrodynamic radius $R_h^{poly}$, solution correlation length, $\xi$, and $C_{60}$ cluster $R_C$. From a practical standpoint, understanding the equilibrium and nonequilibrium properties of fullerenes and their derivatives is important to applications ranging from plastic electronics[3] to cosmetics.[18]

## EXPERIMENTAL SECTION

Four representative isopleths of this ternary system are studied: two in a dilute solution regime and two in the semidilute regime, summarized in Figure 1 and Table 1. Five PS molecular weights $M_w$ = 20, 65, 79, 100, and 1000 kg mol$^{-1}$ and polydispersity indices (PDI) ranging from 1.05 to 1.15 (referred to hereafter as 20k, 65k, 79k, 100k, and 1M) were investigated, with concentrations ranging from 0.12 to 9.5 wt %. All deuterated and hydrogenous polymers were purchased from Polymer Source, except 65k PS-h, which was purchased from Polymer Laboratories Ltd. Toluene (99.5%) was purchased from VWR and toluene-$d_8$, used for SANS experiments, from Goss Scientific. $C_{60}$ (99% purity, Mer Corp.) concentrations ranged from 0.005 to 0.96 wt %, below and above the miscibility of $C_{60}$ in toluene ($c_{C_{60}/tol}$) of 0.32 wt %.[17] $C_{60}$ All concentrations ($c_i$) reported are given by the ratio of the mass of component $i$ to the total mass of the solution. Ternary solutions were carefully prepared to avoid inadvertent fullerene aggregation.[19] (Detailed procedure and recommendations are provided in the Supporting Information).

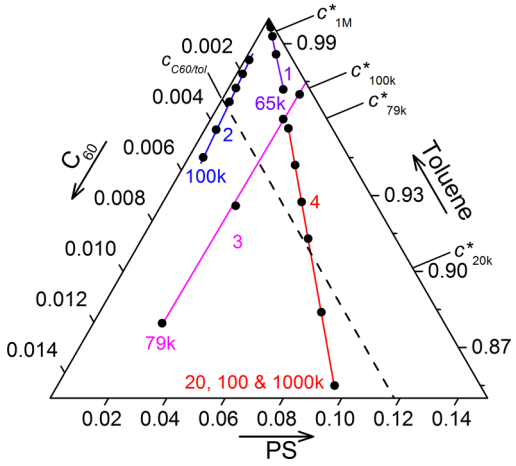


**Figure 1.** Ternary diagram of PS/$C_{60}$/toluene showing the isopleths of mixtures investigated. $c^*$ for PS/toluene is indicated for selected molecular weights. All experiments with PS 65k were in the dilute regime thus $c^*$ is not shown. PS/toluene binary mixtures are not shown for clarity. The black dashed line represents the miscibility limit ($c_{C_{60}/tol}$) of $C_{60}$ in toluene (0.32 wt %).[17]

**Table 1. Summary of Isopleths Investigated, Referenced by Polystyrene $M_w$, Solution Regime, Objective of Isopleth and Technique Used**[a]

| isopleth | $M_w$/kg mol$^{-1}$ | objective | technique |
|---|---|---|---|
| 1 | 65 | dilute regime ($c < c^*$), $C_{60}$:PS = 0.05, $c_{C_{60}} < c_{C_{60}/tol}$ | SLS, DLS |
| 2 | 100 (orange □) | dilute regime ($c < c^*$), $C_{60}$:PS = 1, $c_{C_{60}} < c_{C_{60}/tol} < c_{C_{60}}$ | SANS |
| 3 | 79 (blue △) | semidilute regime ($c \approx c^*$), $c_{C_{60}} < c_{C_{60}/tol} < c_{C_{60}}$ | SANS |
| 4 | 20 (black △); 100 (red ○ or blue □); 1000 (green ◇) | semidilute regime ($c \gtrsim c^*$), $M_w$, $C_{60}$:PS = 0.05, $c_{C_{60}} < c_{C_{60}/tol} < c_{C_{60}}$ | SANS |

[a]Concentrations of individual samples can be found in Table S1 of the Supporting Information.

Isopleth 1, in the dilute solution regime, was investigated by a combination of SLS and DLS, employing cylindrical quartz cuvettes (Hellma) with a diameter of 20 mm as scattering cells. Prior to any measurement, the cuvettes were cleaned from dust by continuously injecting freshly distilled acetone from below for 5 min. Both the SLS and DLS experiments were performed with a CGS-3/MD-8 Compact Goniometer System from ALV, Langen, Germany. The instrument is equipped with an array of eight detectors, where the angle between adjacent detectors is 8°. Each detector comprises an avalanche photodiode and a photocorrelator, allowing the static scattering intensity and the intensity correlation to be recorded simultaneously over an angular range of 56°. The array of detectors as a whole can be rotated around the goniometer between a $\theta_{min}$ of 20° for the leftmost detector and a $\theta_{max}$ of 136° for the rightmost detector. A He−Ne laser from Soliton with a wavelength of $\lambda$ = 632.8 nm was used as light source. The refractive index of the solvent, $n$, in this case toluene, is 1.496. The accessible wavenumber $q$ range, where $q \equiv (4\pi n/\lambda)\sin(\theta/2)$, is thus $5.1 \times 10^{-3} \le q \le 2.7 \times 10^{-2}$ nm$^{-1}$. SANS experiments were carried out with rectangular or banjo Hellma cells (1, 2, or 5 mm depending on the volume of deuterated component) at LOQ (ISIS, Didcot), D11 and D22 (ILL, Grenoble) with $q$-ranges of 0.09−4.85 nm$^{-1}$ (LOQ), 0.013−3 nm$^{-1}$ (D11), and 0.0296−3 nm$^{-1}$ (D22) respectively. Rheology measurements were carried out with an Anton Paar stress controlled rheometer (Physica MCR 301) using a double gap geometry from a shear rate of 200 to 700 s$^{-1}$. All samples exhibited Newtonian behavior. All experiments on SLS, DLS, and SANS and rheology were carried out at 25 °C.

## SCATTERING THEORY AND ANALYSIS

Static light scattering (SLS) measured the excess Rayleigh ratio of the solute,

$$R(q) = \frac{S_{sample}(q) - S_{solvent}(q)}{S_{standard}(q)} R_{standard} \quad (1)$$

where $S_{sample}(q)$ and $S_{solvent}(q)$ are the measured scattering signals of the sample and solvent and $S_{standard}(q)$ and $R_{standard}$ are the scattering signal and the known Rayleigh ratio of the standard (toluene). $S_{sample}(q)$ also takes into account the light absorption of $C_{60}$ via a multiplicative term $(T_{solvent} - T_{background})/(T_{sample} - T_{background})$. SLS experiments were employed to determine the size of the scattering objects in terms of a $z$-averaged radius of gyration, $R_g$. Scattering curves with low angular dependence were evaluated by means of the Zimm approximation:[20]

$$\frac{1}{R_{(q)}} = \frac{1}{R_0}\left(1 + \frac{q^2 R_g^2}{3}\right) \quad (2)$$

$$\frac{Kc}{R_{(q)}} = \frac{1}{M_w} + \frac{R_g^2 q^2}{3M_w} + 2A_2 c \quad (3)$$

$$K = \frac{4\pi^2 n^2}{N_A \lambda^4}\left(\frac{dn}{dc}\right)^2 \quad (4)$$

From eq 2, the $R_g^2$ of the dissolved components and the Rayleigh ratio at zero scattering angle, $R_0$, can be determined by a linear fit to a plot of $1/R_{(q)}$ versus $q^2$, which is valid


dx.doi.org/10.1021/ma501015s | Macromolecules XXXX, XXX, XXX−XXX

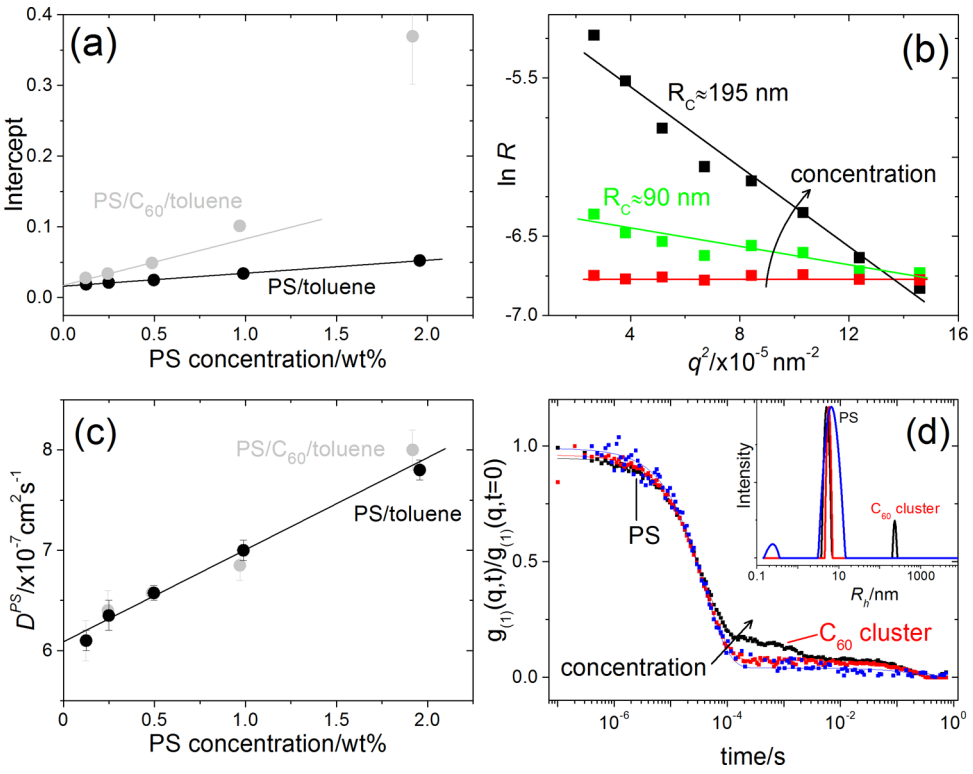


**Figure 2.** Results from static and dynamic light scattering measurements of PS/toluene and PS/$C_{60}$/toluene along isopleth 1. (a) Extrapolation of the intercepts from Zimm plots (Figure S2, Supporting Information) for PS/tol (black) and PS/$C_{60}$/tol (gray) to zero concentration. For the higher concentrations of $C_{60}$ only the high $q$ portion of the data was extrapolated to zero. The intercept at zero concentration gives $1/M_w$, which with and without $C_{60}$ yields polymer $M_w$ = 61.3 kg/mol, in agreement with the expected 65 kg/mol. (b) Guinier plot of low $q$ scattering. $R_C$ values of 195 ± 25 nm and 90 ± 10 nm are fitted for PS concentrations of 1.93 (black) and 0.97 wt % (green), respectively, arising from $C_{60}$ aggregation; we note that this is *below* $c_{C_{60}/tol}$. No aggregation is observed at 0.49 wt % (red). (c) Extrapolation to zero concentration of fitted diffusion coefficients (Figure S3, Supporting Information) for isopleth 1 showing PS/toluene (black) and PS/$C_{60}$/toluene (gray). As shown by the black line, there is no change in the polymer diffusion coefficient upon addition of $C_{60}$, corresponding to $R_h^{PS}$ of 6.45 nm. (d) Correlation functions, at $\theta$ = 80° ($q$ = 0.019 $nm^{-1}$), at three concentrations, 0.12 wt % PS (blue), 0.49 (red), and 1.93 (black). Solid lines are fits to the data using eq 8. The inset shows the result of the corresponding CONTIN analysis. A second decay emerges for 1.9 wt % PS, with an $R_h^{cluster}$ in the region of 200 nm, following 12 h of sample preparation.

independently of particle shape for $qR_g \leq 1$. Additionally, the polymer $M_w$ and second osmotic virial coefficient ($A_2$) can be computed using eq 3. The contrast factor, $K$, is defined in eq 4 where $N_A$ and $dn/dc$ are Avogadro's number and refractive index increment of the polymer/solvent system. However, a Zimm analysis of scattering curves of large particles yields large slopes $R_g^2/(3R_0)$ and intercepts $1/R_0$ close to zero, which causes significant experimental uncertainties. Therefore, a Guinier approximation[21] (eq 5) is best suited to extract $R_g$ from strongly angular-dependent scattering curves, as observed in some mixtures below. We note that light scattering from molecularly dispersed $C_{60}$ in solution did not exhibit angular dependent scattering. In general, Zimm analysis effectively yielded $R_g^{poly}$ and Guinier analysis provided $R_C$ of fullerene clusters.

$$\ln R(q) = \ln R_0 - \frac{q^2 R_g^{\,2}}{3} \tag{5}$$

The intensity correlation $g^{(2)}(t)$ obtained from dynamic light scattering (DLS) was transformed into the field correlation function $g^{(1)}(t)$ by means of the Siegert relation.[22] The field correlation function $g^{(1)}(t)$ was treated in two alternative ways. According to the cumulant analysis,[23] a plot of $\ln(g^{(1)}(t))$ versus relaxation time, $t$, was analyzed for short $t$ according to

$$\ln(g^{(1)}(q,t)) = G - \Gamma(q,c)t + \frac{\mu_2}{2\Gamma^2(q,c)}t^2 \tag{6}$$

where $G$ is a constant and $\Gamma(q,c)$ is the mean inverse relaxation time of diffusive modes, with $z$-average translational diffusion coefficient $D(q,c) = \Gamma(q,c)/q^2$, and $c$ is the mass concentration of the solute. The quantity $\mu^2/\Gamma^2(q,c)$ corresponds to the normalized variance of the intensity-weighted distribution of diffusion coefficients and is used as a fitting parameter only. Linear extrapolation of $D(q,c)$ toward $q^2 \to 0$ and $c \to 0$ yields $D_0$, corresponding to zero scattering angle and infinite dilution, from which a mean effective hydrodynamic radius $R_h$ of the PS coils or $C_{60}$ clusters is computed from the Stokes–Einstein equation:

$$R_h = \frac{k_B T}{6\pi\eta D_0} \tag{7}$$

where $k_B$ is the Boltzmann constant, $T$ is the temperature, and $\eta$ is the dynamic viscosity of the solvent. The cumulant analysis was used to extract the hydrodynamic radius from a monomodal field correlation function. For the case of two or three well-resolved modes, $g^{(1)}(t)$ was modeled with double- or triple-exponentials ($N$ = 2 or 3), allowing a statistically robust estimate of the $z$-average particle size and corresponding partial scattering intensity of the respective mode:


dx.doi.org/10.1021/ma501015s | *Macromolecules* XXXX, XXX, XXX–XXX

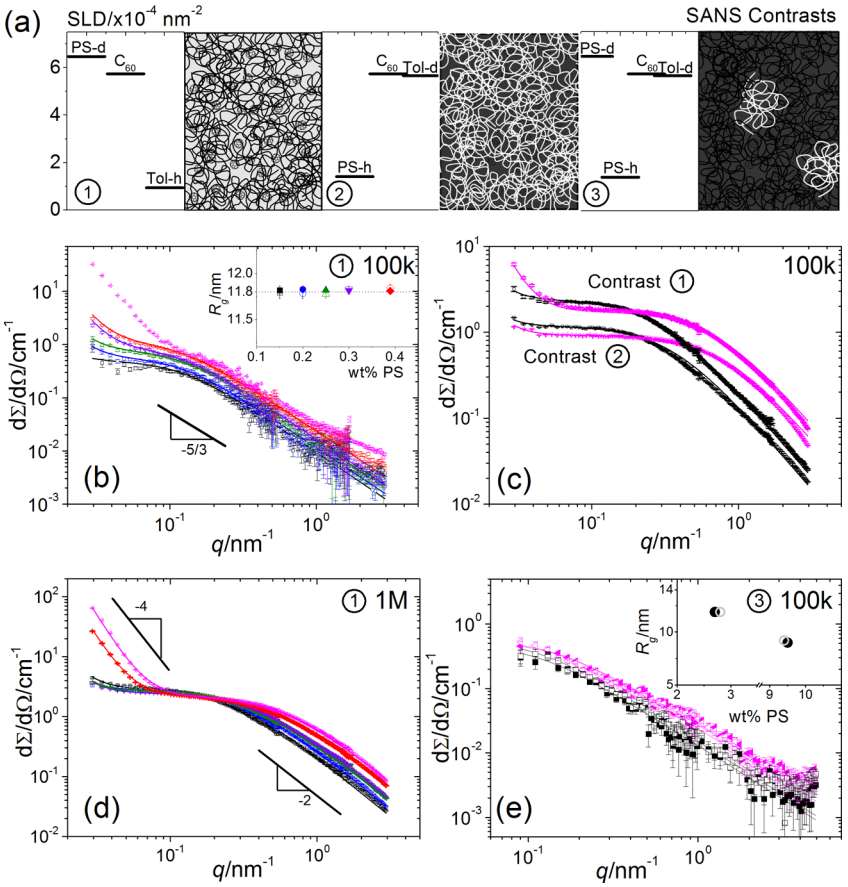


**Figure 3.** (a) Schematic of the three SLD contrasts used: contrast ① (PS-d/$C_{60}$/Tol-h), ② (PS-h/$C_{60}$/Tol-d) and ③ (PS-d/PS-h/$C_{60}$/Tol-h). (b)−(e) Coherent SANS intensity for isopleths 2 and 4. The contrast used is indicated. $C_{60}$ = 0.15 (□), 0.2 (○), 0.25 (△), 0.3 (▽), 0.4 (◇), and 0.5 (◁) wt %. (b) 100k PS-d/$C_{60}$/tol-h along Isopleth 2 ($C_{60}$:PS = 1). The inset shows fitted $R_g$ (11.7−11.8 nm) for PS/$C_{60}$/toluene (hollow symbols) and PS/toluene (filled symbols), the dashed line is calculated using $R_g$ [nm] = 1.25 × 10$^{-5}$$M_w^{0.595}$. (c)−(e) correspond to isopleth 4 ($C_{60}$:PS = 0.05). (c) Comparison of contrasts ① and ② demonstrates the low $q$ upturn was due to scattering contributions from $C_{60}$ at 0.15 and 0.5 wt % $C_{60}$. (d) 1M PS with power laws indicated. Solid lines in (c) and (d) are fits to eq 9. (e) 100k PS-d/PS-h/$C_{60}$/toluene using contrast ③ to evaluate the effect of $C_{60}$ on single chains taken at either end of isopleth 4 (0.15 (□) and 0.5 (◁) wt % $C_{60}$). Neat PS-d/PS-h/Tol-d (filled symbols) included for comparison. Solid lines are data fits using the PolymerExclVolume model.[25] The inset shows fitted $R_g^{PS}$ with total concentration of PS (h and d) for systems with (○) and without $C_{60}$ (●) in the semidilute regime.

$$g^{(1)}(q,t) = \sum_{i=1}^{N} a_i(q)\exp(-\Gamma_i(q)t) \tag{8}$$

where each coefficient $a_i(q)$ represents the intensity-weighted contribution of the respective $\Gamma_i(q)$ to the distribution of diffusive modes; for a large numbers of exponentials ($N \geq 50$), eq 8 can be solved by means of the CONTIN analysis.[24]

Small angle neutron scattering (SANS) was employed to probe polymer conformation, fullerene clustering, and composition fluctuations in the mixtures. The total scattering intensity, $I(q)_{tot}$ was background-subtracted to give the coherent scattering intensity, $I(q)_{coh}$, by using the appropriate fraction of hydrogenous component, solvent or polymer, which was then fit using SasView (v2.2.0).[25] In the dilute regime (isopleth 2), PS solution scattering was analyzed with the well-known polymer excluded volume model (PolymerExclVol in SasView[26]). Semidilute solutions (isopleths 3 and 4) were analyzed by an Ornstein−Zernike (OZ) form with a Porod contribution (CorrLength in SasView[27]):

$$I(q)_{coh} = Aq^{-4} + \frac{B}{1 + (q\xi)^2} \tag{9}$$

because the scattering contribution from $C_{60}$ clusters appears at low $q$ values and is effectively decoupled from $S_{poly}(q)$, both in the dilute and in the semidilute regimes. Here $A$ is used solely as a weighting factor which is fit alongside the $R_g$ or $\xi$ of the PS in solution. The scattering from $C_{60}$/toluene binary solutions $\lesssim$1 wt % is featureless in this $q$ range.

Three different scattering length density (SLD) contrasts were used (illustrated later in Figure 3a), defined by $(\rho N_A/M)\sum b_i n_i \times 10^5$ where $b_i$, $n_i$, $M$, and $\rho$ are atomic scattering length of atom $i$ [fm], number of $i$ atoms, monomer mass [g/mol], and density [g/cm$^3$]. For this system, SLD = 1.41 (PS-h), 6.47 (PS-d), 5.73 ($C_{60}$), 0.94 (Tol-h), and 5.66 (Tol-d) × 10$^{-4}$ nm$^{-2}$. $C_{60}$ has a SLD similar to that for deuterated toluene, and mixtures of PS-h/$C_{60}$/Tol-d allow the characterization of the polymer PS-h. Contrast ① provides information on both PS and $C_{60}$, whereas scattering with contrasts ② and ③ is dominated by contributions from PS chains. In contrast ②, $\xi$ can be found above $c^*$, whereas with contrast ③, the $R_g$ of single polymer coils in the semidilute regime can be found for sufficiently low PS-h concentration within the overall PS content.


dx.doi.org/10.1021/ma501015s | Macromolecules XXXX, XXX, XXX−XXX

## RESULTS AND DISCUSSION

We first discuss the PS conformation in the dilute solution regime, where $c \ll c^*$, corresponding to isopleths 1 and 2. The overlap concentration is defined as $c^* = 3M_w/4\pi N_A R_g^3$, where $M_w$ is the molecular weight [kg/mol], $N_A$ is Avogadro's constant, $R_g$ [m] is the radius of gyration of a single polymer coil in the dilute limit. In a good solvent, excluded volume interactions lead to chain expansion compared to theta conditions and $R_g \simeq N^\nu$ with $\nu = 0.588$, where $N$ is the number of monomers per chain and $\nu$ is the characteristic scaling exponent.[28] Experimentally, PS in toluene[29] has been found to follow $R_g$ [nm] $= 1.25 \times 10^{-5} M_w^{0.595}$.

Isopleth 1 traverses varying toluene concentrations at a constant ratio of $C_{60}$:PS of 0.05. Zimm analysis of SLS data was carried out for neat PS/toluene solutions (Figure S2a, Supporting Information). A polymer $M_w$ of 65 kg/mol was chosen for this study as there is no angular dependence of PS solution scattering in this $q$ range, which facilitates the identification of fullerene association. The data were used to linearly extrapolate to $q = 0$, within the $q$ range $(5.1-27) \times 10^{-3}$ nm$^{-1}$, yielding a $c = 0$ intercept of 0.0163 ± 0.003, and therefore a $M_w$ of 61.3 ± 1.2 kg/mol, close to the expected 65k. The results are shown in Figure 2a. Along isopleth 1, there was a clear increase in scattering intensity for solutions containing higher loadings of $C_{60}$ (0.04 and 0.09 wt %). Guinier analysis, shown in Figure 2b, indicates scattering from a component with $R_C$ in the region of 100−200 nm after 12 h of solution preparation. Experiments with 20k and 1M PS show similar results, indicating a reduction in $C_{60}$ miscibility with addition of polymer. Extrapolation for PS/$C_{60}$/tol (Zimm plot shown in Figure S2b of the Supporting Information) to $c = 0$ is also shown in Figure 2a, yielding the same intercept as for PS/tol solutions and therefore same polymer $M_w$. However, the slope is clearly different; the $A_2$ calculated for PS/toluene is 0.008 cm$^3$ mol g$^{-2}$, in good agreement with the literature.[30] The change in gradient upon $C_{60}$ addition, shown in Figure 2a, can be due to two factors: changes in $A_2$ and d$n$/d$c$ of $C_{60}$/toluene. Because $A_2$ is a binary interaction parameter relating to the interaction of PS and toluene, and polymer dimensions remain unchanged with $C_{60}$ addition (see isopleths 2−4), we expect the observed change in slope to be due to changes in d$n$/d$c$ of $C_{60}$/toluene (such measurements are, however, complex and outside the scope of this paper).

DLS of the same solutions generally corroborate the conclusions above. Extrapolations to $q = 0$ and $c = 0$ of the PS 65k diffusion coefficient with and without $C_{60}$ are shown in Figure 2c. The same diffusion coefficient is found in both cases, $D = 6.08 \times 10^{-7}$ cm$^2$ s$^{-1}$, in agreement with previous work.[29] The solution viscosity remained constant within experimental uncertainty for $C_{60}$ concentrations from 0 to 0.3 wt % in toluene ($\eta$ = 0.608−0.631 mPa s). An unchanged $R_h^{PS}$ = 6.45 nm is obtained from eq 7 upon the addition of $C_{60}$, within measurement error. Selected DLS data for the same $q$ range is shown in Figure 2d for PS/$C_{60}$/toluene with fitted correlation functions from eq 8 where $i = 1-3$, depending on the number of decays observed. A component corresponding to individual $C_{60}$ molecules cannot be reliably extracted. The correlation function for the ternary blend with the highest PS concentration (1.9 wt % PS and 0.09 wt % $C_{60}$) shows a clear second decay corresponding to a peak at 200 nm via CONTIN analysis, which we associate with fullerene aggregates also observed by SLS. The $R_h^{C_{60}}$ is in good agreement with the $R_C$ estimate from the Guinier plots (Figure 2b). These results demonstrate a decrease of $C_{60}$ miscibility in toluene upon the addition of PS.

$C_{60}$ aggregates of 100−200 nm present in PS/$C_{60}$/toluene blends of sufficiently high PS concentrations ($\gtrsim$0.5 wt % 65k PS), in addition to unperturbed PS chains and individual fullerene molecules in toluene. We have found that cluster sizes increase with time and the macroscopic sedimentation is eventually observed after a period of days. Due to experimental limitations associated with light absorption, higher concentrations of $C_{60}$ cannot be reliably measured via light scattering. SANS was therefore employed for $C_{60}$ concentrations above $c_{C_{60}/tol}$.

SANS data from isopleth 2 ($C_{60}$:PS = 1) is shown in Figure 3b. Contrast ① (PS-d, $C_{60}$, and Tol-h) was chosen, such that scattering is dominated by contributions from PS and $C_{60}$ at the expense of a larger incoherent background from tol-h. Along this isopleth, a clear increase in scattering intensity at low $q$-values, from 0.03 to 0.1 nm$^{-1}$, as the concentration of solids increases. Contrast variation experiments discussed below assign this upturn to $C_{60}$ clusters, forming at 0.3−0.5 wt % PS-100k. The high $q$ scaling exponent is expected to be $\nu = 5/3$ for the conformation of a polymer in a good solvent and is found experimentally to range from 1.66 to 1.85 for the samples investigated (in broad agreement, which is, however, sensitive to the background subtraction and ideal mixing assumption). Further, we observe no change in $R_g$ for the samples investigated within error when compared to values for neat 100k PS/toluene (filled symbols in the inset of Figure 3b). An effective Flory−Huggins interaction parameter, $\chi$, was found for the solutions in isopleth 2, 0.44−0.48, in agreement with those previously found in literature for PS/toluene.[31] We can therefore conclude by SLS, DLS, and SANS that there is no change in $R_h^{PS}$, $R_g$, and $\chi$ for PS/$C_{60}$/tol solutions studied in the dilute regime.[32]

We next consider the semidilute regime, for which the concentration of polymer is greater than $c^*$. Semidilute solutions are characterized by a correlation length, $\xi$, of concentration fluctuations and scaling theory predicts a concentration dependence of $\xi \propto c^{-\nu/(3\nu-1)}$,[28] so that $\xi \propto c^{-0.77}$ for PS in toluene (using $\nu = 0.588$). This exponent has also been verified experimentally,[33−35] and Brown and Nicolai[33] compiled data for PS in a number of good solvents to find a general scaling $\xi = 0.27 \pm 0.1 \times c^{-0.72\pm0.01}$, where $\xi$ [nm] and $c$ [g/mL], and thus an exponent close to the predicted value of −0.77.[28]

Along isopleth 3 (constant of 2.4 wt % PS and with 0 to 0.96 wt % $C_{60}$), the concentration of $C_{60}$ eventually exceeds $c_{C_{60}/tol}$ and fullerenes precipitate. It has been previously found that high colloidal loadings can result in changes of polymer dimensions[11] in solution. Contrast ② was used in this case (PS-h, $C_{60}$, tol-d) so that potentially small changes in PS conformation could be investigated. The excess low-$q$ scattering, previously observed in Figure 3b is not observed due to $C_{60}$ and tol-d contrast matching, corroborating our assignment to $C_{60}$ clusters. All data superpose for loadings of $C_{60}$ both above and below $c_{C_{60}/tol}$ of 0.32 wt % (Figure S5, Supporting Information). Ornstein−Zernike analysis, according to eq 9, yields unchanged correlation length $\xi$ (ranging from 3.44 to 3.54 nm) for all the solutions in isopleth 3, within measurement uncertainty.


dx.doi.org/10.1021/ma501015s | Macromolecules XXXX, XXX, XXX−XXX

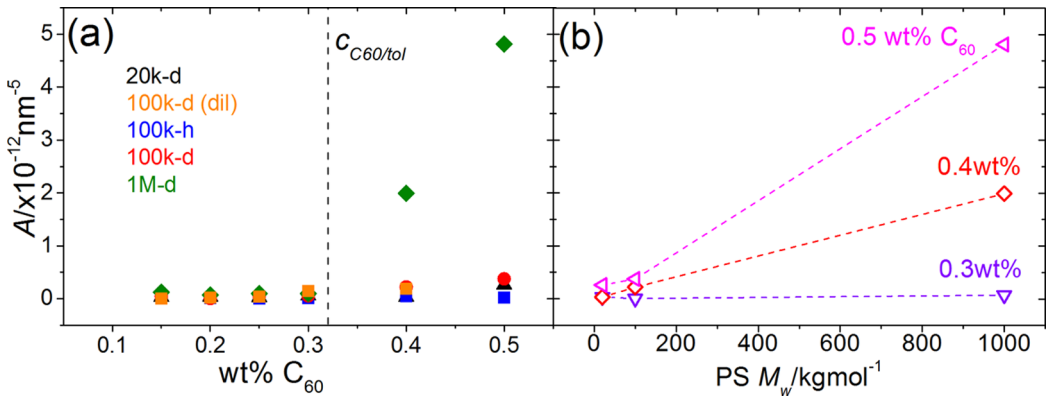


**Figure 4.** Weighting factor, $A$, for the three molecular weights (20k, 100k, and 1M) studied on isopleth 2 and 4. (a) The dashed black line indicates $c_{C_{60}/tol}$ of $C_{60}$ in toluene (0.32 wt %)[17] The values for $A$ from the dilute 100k-d PS (100k-d dil) obtained in isopleth 2 are also included. The data for 100k-h is included as a baseline for which the $C_{60}$ aggregation is not observed due to contrast matching. The inset in (a) focuses on the region below $c_{C_{60}/tol}$. (b) $A$ as a function of $M_w$ for isopleth 4, at $C_{60}$ = 0.3 (▽), 0.4 (◇), and 0.5 (◁) wt %.

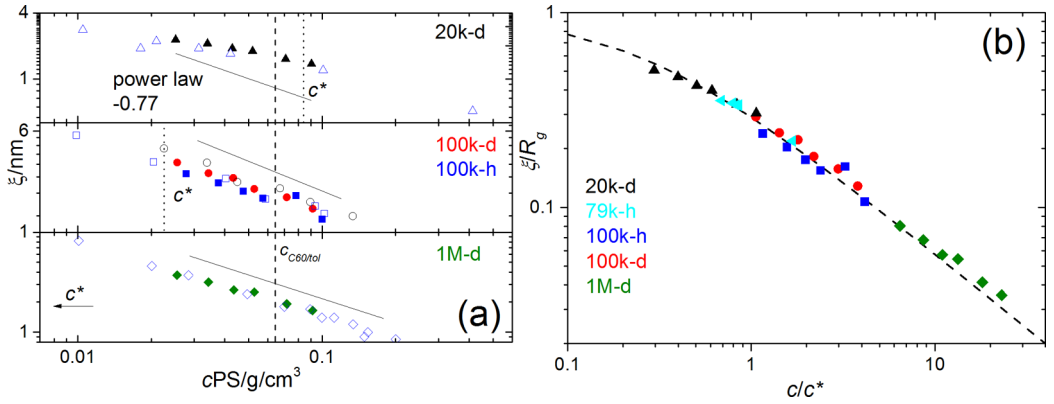


**Figure 5.** (a) Fitted correlation length $\xi$ against PS concentration in the overall PS/$C_{60}$/toluene solution for isopleth 4 ($C_{60}$/:PS = 0.05) for the three $M_w$ studied (filled symbols).The hollow symbols are literature data for $M_w$ from King et al.[34] (100 kg/mol, black) and Hamada et al.[35] (17.5, 110, and 900 kg/mol, blue). Dashed lines indicate $c^*$ for the 20k and 100k. $c^*$ for 1M is not on this scale, as indicated by the arrow. (b) Reduced correlation length $\xi/R_g$ of data from both isopleths 3 and 4 in the semidilute regime, covering a regime of $C_{60}$:PS from 0 to 0.41 and $C_{60}$ loading from 0 to 0.96 wt % plotted against reduced concentration $c/c^*$. A line of best fit of the form $(1 + \beta c/c^*)^{\alpha}$, where $\beta = 4$ and $\alpha = -0.77$.[39] $R_g$ was calculated using $R_g$ [nm] = 1.25 × 10$^{-5}$$M_w^{0.595}$.

Isopleth 4 exceeds $c_{C_{60}/tol}$ and, to elucidate the $C_{60}$ scattering contribution, contrast ① was used. This enables fullerene aggregation, seen previously with SLS and DLS in dilute systems, to be observed in the semidilute regime. Previous literature has suggested that up to 1 wt %[36] or 3 wt %[37] $C_{60}$ is miscible in PS melts. In solution, depending on the relative component miscibility it could be expected that either (i) PS suppresses $C_{60}$ aggregation due to improved solvent quality or (ii) unfavorable interactions result in polymer:fullerene phase separation in solution. Figure 3c compares the coherent scattering signals from contrasts ① and ② at fixed $M_w$ (100k). The upturn seen with contrast ① can unambiguously be attributed to $C_{60}$ by contrast variation. Figure 3d shows the background subtracted and fitted data for 1M PS (20k and 100k shown in Figure S6, Supporting Information). A scaling of −4 indicates sharp interfaces, and parameter $A$ is used a qualitative indicator of the magnitude of fullerene aggregation, via the extent of forward scattering. A third contrast matching experiment was carried out, using contrast ③ at either end of isopleth 4 with PS-100k. However, a low concentration of PS-h (0.110 ± 0.003 wt %) in the overall ternary/quaternary mixtures is employed, much less than $c^*$ of 2.8 wt % for 100k PS and thus allowing the direct determination of single chain polymer conformation in semidilute solutions ($c_{PS\text{-}h} + c_{PS\text{-}d} > c^*$). As found in Figure 3e, no polymer $R_g$ change is observed upon addition of 0.15 and 0.5 wt % $C_{60}$. The values of the fitted $R_g$ agree with those of King et al.[34] and Daoud et al.[38] who characterized the dependence of $R_g$ of PS in toluene with concentration in the semidilute regime.

There is a clear $M_w$ dependence in the low-$q$ scattering intensity, increasing from 20k to 1M, and Figure 4a plots the weighting factor, $A$, as a function of wt % $C_{60}$. Figure 4b shows that 1M PS, along isopleth 4, exhibits the greatest $A$ at constant mass fraction. $A$ for dilute 100k PS from isopleth 2 is also included in Figure 4a and is found to take similar values for 100k PS regardless of whether in the dilute (orange square) or semidilute (red circle) regime. $C_{60}$ cluster dimensions, shape, or number cannot be extracted from the SANS data in this $q$ range. However, SLS and DLS data on the addition of PS in the dilute regime induced $C_{60}$ aggregation of 100−200 nm. According to the Asakura−Oosawa model,[5,6] the depletion layer around colloidal particles is governed by the polymer $R_g$. Thus, as $R_g$ increases from 4.5 to 46 nm, corresponding to $M_w$ from 20k to 1M, the depletion layer around $C_{60}$ aggregates should increase accordingly. Although the model applies only within the dilute solution regime, it provides qualitative insight


dx.doi.org/10.1021/ma501015s | Macromolecules XXXX, XXX, XXX−XXX

**Scheme 1. Schematic Depicting the Presence of Fullerene Clusters (10−100 nm) alongside Individual $C_{60}$ Molecules and Undisturbed Polystyrene Chains[a]**

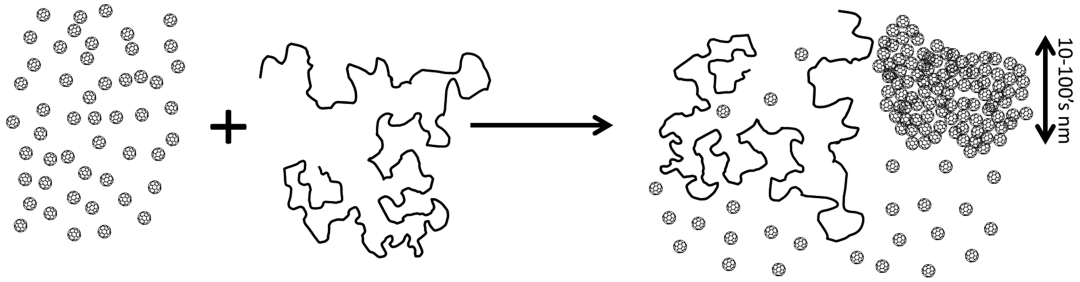


[a]Fullerene agglomeration occurs for sufficiently large polymer $M_w$ at constant mass fraction.

into these observations. Indeed, upon increasing polymer $M_w$, $C_{60}$ aggregates should experience a greater anisotropic osmotic pressure gradient, contributing to further aggregation, as confirmed by the increased forward scattering intensity observed experimentally. This result is surprising, as above $c^*$ one should not expect a $M_w$ effect on solution conformation. This could, however, be related to the very broad crossover between dilute and semidilute regimes, which in turn may impact the degree of solution homogeneity for the various polymer $M_w$. Evidently, the larger the $M_w$ at constant mass fraction, the further away the solution is from the crossover definition.

The fitted correlation lengths $\xi$, shown in Figure 5a, agree almost perfectly, with the results obtained by King et al.[34] and Hamada et al.[35] for PS/toluene solutions. The lower $M_w$ 20k PS data deviate from the scaling law of −0.77, unlike those of 100k and 1M. This is, however, expected because the concentrations studied being are lower than $c^*$ for this $M_w$ (the semidilute crossover is, however, broad and solutions display semidilute properties across this range[33,40]). We conclude, similarly to the dilute regime, that the polymer conformation in the semidilute regime remains unchanged below and above $c_{C_{60}/tol}$. The fitted $\xi$ for isopleths 3 and 4 also fall onto a master curve with the correlation length reduced by a constant $R_g$, calculated using $R_g$ [nm] = $1.25 \times 10^{-5} M_w^{0.595}$,[29] and concentration reduced by $c^*$, shown in Figure 5b. A functional form $\xi/R_g = (1 + \beta c/c^*)^{\alpha}$, where $\alpha = -0.77$, the expected exponent for semidilute polymer solutions in a good solvent, is found to accurately describe all results.[39]

## CONCLUSIONS

In summary, we have investigated the conformation and interactions of polystyrene, and the dispersion of fullerenes, in ternary solutions with toluene. Given the limited miscibility of $C_{60}$ in pure toluene (0.32 wt %), only fullerene concentrations between 0 and 0.96 wt % were studied. We have shown that the $R_h$ and $R_g$ for PS in dilute solutions (isopleths 1 and 2) are unchanged upon addition of $C_{60}$. Further there is no change in the solvent quality experienced by PS chains in the concentration range measured for PS (0.12−1.93 wt %) and $C_{60}$ (0.005−0.5 wt %) and $R_g$ follows the expectation for neat PS/toluene solutions. The correlation length $\xi$ in PS/toluene solutions, for which PS is in the semidilute regime (isopleths 3 and 4), is also unchanged by $C_{60}$ addition. Using contrast matching, we find that the $R_g$ of individual chains in a semidilute solutions is also unchanged. The reduced correlation lengths fall onto a master curve with concentration with power law of −0.77 regardless of $C_{60}$ addition up to 0.96 wt % (Figure 5b). Collectively, our results demonstrate that there is no change in PS/toluene solution conformation when $C_{60}$ is added to the system across the various solution regimes. However, the findings are not inconsistent with previous observations[11,12] of a decrease in PS chain dimensions with colloid addition as it is possible that the low solubility limit of $C_{60}$ prevents reaching high enough concentrations ($\gtrsim$8 wt %) to induce coil shrinkage by depletion in the PL.

By contrast, the addition of PS to $C_{60}$/toluene is found to reduce the fullerene miscibility and induce $C_{60}$ aggregation. This is interpreted as due to a reduction in volume available to $C_{60}$ molecules in toluene by addition of the polymer, thus increasing its effective concentration toward $c_{C_{60}/tol}$ (0.32 wt %); $c_{C_{60}/tol}$ clearly decreases by the addition of PS, in particular for higher $M_w$. The Porod exponent of 4 suggests the formation of compact clusters with sharp interfaces. The agglomeration of $C_{60}$ in 100−200 nm aggregates departs from solely being in the PL to between the PL and CL regimes. $C_{60}$ is found to aggregate, at concentrations as low as 0.04 wt % $C_{60}$, well below the $c_{C_{60}/tol}$ for $C_{60}$ in toluene of 0.32 wt %[17] for 0.97 wt % 65k PS.

Our conclusions are qualitatively summarized in Scheme 1. Our findings elucidate, for the first time, the phase behavior and chain conformation in model polymer solutions upon addition of $C_{60}$. Fullerenes and derivatives are ubiquitous in solution processable plastic electronics and the latter evidently experience complex morphological transitions during drying and film formation.[3]

## ASSOCIATED CONTENT

### Supporting Information

Exact concentrations of PS/$C_{60}$/toluene solutions used in isopleths 1−4 are tabulated, alongside notes regarding sample preparation. Zimm plots and results from SLS and DLS for dilute solutions from isopleth 1 of PS/toluene and PS/$C_{60}$/toluene are shown. SANS spectra from isopleth 3 and 4 are shown with fits. This material is available free of charge via the Internet at http://pubs.acs.org/.

## AUTHOR INFORMATION

### Corresponding Author

*J. T. Cabral. E-mail: j.cabral@imperial.ac.uk.

### Notes

The authors declare no competing financial interest.

## ■ ACKNOWLEDGMENTS

The authors thank the Engineering and Physical Sciences Research Council (EPSRC) for funding (EP/G037515/1) and ILL, Grenoble, France and ISIS, Didcot, U.K. for beamtime and Ann Terry (ISIS, Didcot, UK) for support. AJN acknowledges partial support by an Imperial College Junior Research Fellowship and from a Royal Society Research Grant (RG110374). We thank Jack F. Douglas for useful discussions. This work benefitted from SasView software, originally developed by the DANSE project under NSF award DMR-0520547.

## ■ REFERENCES

(1) Keddie, J.; Routh, A. F. *Fundamentals of Latex Film Formation - Processes and Properties*; Springer Laboratory; Springer: Berlin, 2010.
(2) Böker, A.; He, J.; Emrick, T.; Russell, T. P. *Soft Matter* **2007**, *3*, 1231.
(3) Thompson, B. C.; Fréchet, J. M. J. *Angew. Chem. (Int. Ed. Engl.)* **2008**, *47*, 58−77.
(4) Lekkerkerker, H. N.; Tuinier, R. *Colloids and the Depletion Interaction*; Lecture Notes in Physics; Springer: Berlin, 2011; Vol. *833*.
(5) Vrij, A. *Pure Appl. Chem.* **1976**, *48*, 471−483.
(6) Asakura, S.; Oosawa, F. *J. Chem. Phys.* **1954**, *22*, 1255.
(7) Mutch, K. J.; van Duijneveldt, J. S.; Eastoe, J. *Soft Matter* **2007**, *3*, 155.
(8) de Gennes, P. G. *Compt. Rend. Acad. Sci.* **1979**, *288*, 359−361.
(9) Odijk, T. *Macromolecules* **1996**, *29*, 1842−1843.
(10) (a) Sear, R. *Phys. Rev. E* **1998**, *58*, 724−728. (b) Schoot, P. V. D. *Macromolecules* **1998**, *31*, 4635−4638.
(11) Kramer, T.; Scholz, S.; Maskos, M.; Huber, K. *J. Colloid Interface Sci.* **2004**, *279*, 447−57.
(12) (a) Kramer, T.; Schweins, R.; Huber, K. *Macromolecules* **2005**, *38*, 151−159. (b) Kramer, T.; Schweins, R.; Huber, K. *Macromolecules* **2005**, *38*, 9783−9793. (c) Kramer, T.; Schweins, R.; Huber, K. *J. Chem. Phys.* **2005**, *123*, 014903.
(13) Polson, A.; Potgieter, G.; Largier, J.; Mears, G.; Joubert, F. *Biochim. Biophys. Acta* **1964**, *82*, 463−475.
(14) (a) Nakatani, A. I.; Chen, W.; Schmidt, R. G.; Gordon, G. V.; Han, C. C. *Polymer* **2001**, *42*, 3713−3722. (b) Sen, S.; Xie, Y.; Kumar, S.; Yang, H.; Bansal, A.; Ho, D.; Hall, L.; Hooper, J.; Schweizer, K. *Phys. Rev. Lett.* **2007**, *98*, 128302. (c) Tuteja, A.; Duxbury, P. M.; Mackay, M. E. *Phys. Rev. Lett.* **2008**, *100*, 77801. (d) Jouault, N.; Dalmas, F.; Said, S.; Di Cola, E.; Schweins, R.; Jestin, J.; Boué, F. *Macromolecules* **2010**, *43*, 9881−9891. (e) Crawford, M. K.; Smalley, R. J.; Cohen, G.; Hogan, B.; Wood, B.; Kumar, S. K.; Melnichenko, Y. B.; He, L.; Guise, W.; Hammouda, B. *Phys. Rev. Lett.* **2013**, *110*, 196001.
(15) Kroto, H. W.; Heath, J. R.; O'Brien, S. C.; Curl, R. F.; Smalley, R. E. *Nature* **1985**, *318*, 162−163.
(16) Sun, Y.-P.; Ma, B.; Bunker, C. E.; Liu, B. *J. Am. Chem. Soc.* **1995**, *117*, 12705−12711.
(17) Ruoff, R. S.; Tse, D. S.; Malhotra, R.; Lorents, D. C. *J. Phys. Chem.* **1993**, *97*, 3379−3383.
(18) http://www.solennebv.com/combray.htm. Accessed July 2013.
(19) (a) Ying, Q.; Marecek, J.; Chu, B. *Chem. Phys. Lett.* **1994**, *219*, 214−218. (b) Wong, H. C.; Higgins, A. M.; Wildes, A. R.; Douglas, J. F.; Cabral, J. T. *Adv. Mater.* **2012**, *25*, 985−991.
(20) Zimm, B. H. *J. Chem. Phys.* **1948**, *16*, 1093.
(21) Guinier, A.; Fournet, G. *Small-angle scattering of X-rays*; Structure of matter series; Wiley: New York, 1955.
(22) Siegert, A. J. F. *On the Fluctuations in Signals Returned by Many Independently Moving Scatterers*; Report; Massachusetts Institute of Technology. Radiation Laboratory: Cambridge, MA, 1943; Vol. *465*.
(23) Koppel, D. E. *J. Chem. Phys.* **1972**, *57*, 4814−4820.
(24) Provencher, S. W. *Comput. Phys. Commun.* **1982**, *27*, 213−227.
(25) SasView, http://www.sasview.org/.
(26) Hammouda, B. *Adv. Polym. Sci.* **1993**, *106*, 87−133.
(27) Hammouda, B.; Ho, D. L.; Kline, S. R. *Macromolecules* **2004**, *37*, 6932−6937.
(28) de Gennes, P. G. *Scaling Concepts in Polymer Physics*; Cornell University Press: Ithaca, NY, 1979.
(29) Huber, K.; Bantle, S.; Lutz, P.; Burchard, W. *Macromolecules* **1985**, *18*, 1461−1467.
(30) Huber, K.; Burchard, W.; Akcasu, A. Z. *Macromolecules* **1985**, *18*, 2743−2747.
(31) Brandrup, J.; Immergut, E. H.; Grulke, E. A.; Abe, A.; Bloch, D. R. *Polymer Handbook*, 4th ed.; John Wiley & Sons Inc.: New York, 2005.
(32) $\chi$ was found using the RPA,[28] and the form factor for a solvent in this instance was set to unity as is commonly done in the literature.[41]
(33) Brown, W.; Nicolai, T. *Colloid Polym. Sci.* **1990**, *268*, 977−990.
(34) King, J. S.; Boyer, W.; Wignall, G. D.; Ullman, R. *Macromolecules* **1985**, *18*, 709−718.
(35) Hamada, F.; Kinugasa, S.; Hayashi, H.; Nakajima, A. *Macromolecules* **1985**, *18*, 2290−2294.
(36) Wong, H. C.; Sanz, A.; Douglas, J. F.; Cabral, J. T. *J. Mol. Liq.* **2010**, *153*, 79−87.
(37) Mackay, M. E.; Tuteja, A.; Duxbury, P. M.; Hawker, C. J.; Van Horn, B.; Guan, Z.; Chen, G.; Krishnan, R. S. *Science* **2006**, *311*, 1740−1743.
(38) Daoud, M.; Cotton, J. P.; Farnoux, B.; Jannink, G.; Sarma, G.; Benoit, H.; Duplessix, C.; Picot, C.; de Gennes, P. G. *Macromolecules* **1975**, *8*, 804−818.
(39) Freed, K. F. *Renormalization Group Theory of Macromolecules*; Wiley-Interscience: New York, 1987.
(40) Colby, R. H. *Rheol. Acta* **2009**, *49*, 425−442.
(41) Hammouda, B.; Nakatani, A. I.; Waldow, D. A.; Han, C. C. *Macromolecules* **1992**, *25*, 2903−2906.